Preprints of the 21st IFAC World Congress (Virtual)
Berlin, Germany, July 12-17, 2020

Multi-time Scale Control of Dual-Stage Nanopositioning Systems ⋆

Aleksandra Mitrovic * **Milos Milanovic** * **Kam K. Leang** ** **Garrett M. Clayton** *

* *Villanova University, Villanova, PA 19085 USA (e-mail: garrett.clayton@villanova.edu).*
** *University of Utah, Salt Lake City, UT 84112 USA, (e-mail: kam.k.leang@utah.edu)*

Abstract: In this paper, a novel multi-time scale control technique is applied to a serial dual-stage nanopositioning system. Dual-stage nanopositioning systems combine a high-speed, short-range actuator and a low-speed, long-range actuator to achieve long-range and high-speed positioning. This results in a system that has relatively complicated dynamics due to the physical interaction between the two actuators and their different time-scales. In addition, models of these actuators can be ill-conditioned, which can lead to issues with numerical simulations and controller design. These issues make dual-stage nanopositioning systems well suited to multi-time scale control algorithms. In the proposed algorithm, the system is split (decoupled) into a set of subsystems, where each subsystem has an individual time scale and is independently controlled via state feedback. This alleviates the issues associated with ill-conditioning and simplifies controller design. This paper introduces the novel multi-time scale control design concept and its application to single-axis dual-stage nanopositioners – although it can be easily expanded to more complex systems, e.g., multi-axes, nanopositioning devices. The proposed control technique is validated through simulations of an experimentally obtained serially coupled dual-stage nanopositioning model.

Keywords: Modeling, Micro and Nano Mechatronic Systems, Desing Methodologies, Identification and Control Methods, Applications of Mechatronic Principles.

1. INTRODUCTION

In this paper, dual-stage nanopositioner control is achieved through the use of a novel multi-time scale approach. Control of nanopositioning systems has attracted significant attention due to a wide spectrum of applications in nanoscale science and technology (Escareno et al., 2019, Zhang et al., 2018, Fleming, 2011, Butler, 2011, Kalyanam et al., 2012, Horowitz et al., 2007). Recently, dual-stage nanopositioning systems have received serious interest because of their potential to achieve high-precision and high-resolution displacements over long ranges (Wang et al., 2018, Tuma et al., 2014, Ito et al., 2017, Zundert et al., 2018). A typical dual-stage nanopositioning system consists of a low-speed, long-range actuator (LRA), used for long, coarse displacements, combined with a high-speed, short-range actuator (SRA), used for shorter, fine displacements. Because the two actuators are separated in terms of speed (typically by at least an order of magnitude), dual-stage nanopositioning systems are well suited to a multi-time scale approach, as studied in this paper.

Nanopositioning systems present many, well established control difficulties, such as the presence of lightly damped mechanical resonances. These can result in large oscillations, especially when sudden changes in displacement or high frequency inputs are applied as described in Fleming et al., 2014. This problem is exacerbated in dual-stage systems because of actuator cross-coupling, where the resonant response of one actuator (for example the LRA) affects the response of the other (SRA) – note that this is most apparent from the LRA to SRA. Since these resonances are, by design, far from each other in frequency, the state-space representation of such system can result in a poorly-conditioned state-space model. This can cause numerical methods to have difficulty converging to a solution. This issue significantly limits the application of well-know and well-developed modern control techniques, such as state feedback, that require a state-space model representation of a system.

Control algorithms designed for dual-stage nanopositioning systems can be predominantly divided into two categories. The first category includes the algorithms based on classical single-input single-output (SISO) design methodologies where the controller is designed through a sequence of two decoupled SISO designs, (Schroeck et al., 2001, Horowitz et al., 2007). In these methods, system models are represented as a transfer function. The second category includes controllers based on optimal design methodologies

⋆ This material is based upon work supported, in part, by the National Science Foundation Grants No. CMMI 1537983 and 1537722. Any opinions, findings, and conclusions or recommendations expressed in this material are those of the author(s) and do not necessarily reflect the views of the National Science Foundation. The authors thank Dr. Verica Radisavljevic-Gajic for useful suggestions and valuable support.

Copyright lies with the authors

(Rezac et al., 2013). This paper proposes a multi-time scale control approach, which is well-suited for dual-stage systems because of their multi-time scale nature and enables the use of state-space methodologies.

Multi-time scale control addresses issues with realistic representations of large-scale systems which include interconnection and coupling between state variables. Small, but not negligible parasitic parameters in state-space models, such as small masses and moments of inertia, can increase the condition number of a matrix which leads to computational difficulties, as explained in Ojalvo, 1990 and Peters et al., 1978. This implies that the spectrum of the matrix is wide and that there are simultaneous phenomena occurrences with different time-scales. Recently, multi-time scale control techniques developed in Radisavljevic et al., 2019 were applied to systems with three-time scales (Radisavljevic et al., 2017, Milanovic et al., 2020). In essence, this control technique splits (decouples) large systems into a set of smaller subsystems, where each subsystem is controlled independently. By doing so, a numerically ill-conditioned high-order matrix is avoided, allowing control design at a subsystem level with well-conditioned matrices. Within the context of multi-time scale control, the contributions of this paper include:

- A novel control approach for nanopositioning mechatronic systems, where a multi-time scale control technique is applied to a piezoactuated dual-stage nanopositioning system, and
- A composite state feedback construction procedure that uses observed states of each decoupled single time-scale subsystem.

The remainder of this paper is organized as follows: Sec. 2 introduces dual-stage systems and presents the experimentally obtained dual-stage models of the LRA and the SRA used to verify the proposed control algorithm. Sec. 3 describes the multi-time scale controller, followed in Sec. 4 by simulations results. The main results are highlighted and conclusions are offered in Sec. 5.

2. DUAL-STAGE NANOPOSITIONER MODELS

To highlight the issues associated with dual-stage positioner models, a dual-stage system is modeled in the next section, followed by an experimentally obtained dual-stage nanopositioning model.

2.1 Dual-stage Systems Modeling

In order to increase the precision and operational bandwidth of single-stage nanopositioning systems, a second actuator can be added in series or parallel, resulting in what

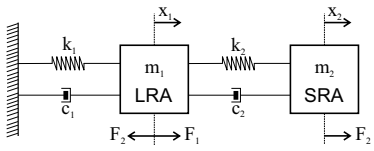

Figure 1. Lumped parameter model of the dual stage nanopositioning system with LRA mass m_1, SRA mass m_2, equivalent stiffness k_1, k_2 and damping coefficients c_1, c_2.

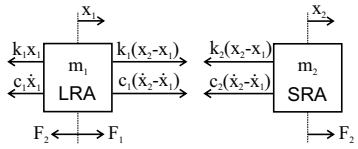

Figure 2. Free body diagram of m_1 and m_2 lumped mass elements.

is commonly referred to as dual-stage actuator system. The modeling and control of dual-stage nanopositioning systems is challenging due to the presence of nonlinearities such as hysteresis and thermal drift. Lightly damped mechanical resonances also present a challenge in that they limit the speed and bandwidth of the system. Mechanical resonances usually arise from the platform mass interaction with the stiffness of support flexures, actuators and mechanical linkages, as described in Fleming et al., 2014.

A schematic example of a serial dual-stage nanopositioning system, on which this paper focuses, is shown in Fig. 1. The actuators are modeled as two lumped mass elements m_1 and m_2, interconnected via two springs k_1 and k_2 and two dampers c_1 and c_2. The inputs to the system are force F_1, from the LRA piezoelectric actuator and the force from the SRA actuator F_2, which moves the second mass and results in a reaction force on the first. The outputs of the system are the LRA displacement x_1 and the SRA displacement measured as $x_2 - x_1$, as shown in Fig. 2.

Based on the free body diagram in Fig. 2, a state-space model of the form

$$\dot{x}(t) = Ax(t) + Bu(t) \tag{1}$$
$$y(t) = Cx(t) + Du(t), \tag{2}$$

was found to be

$$\begin{bmatrix} \dot{x}_1(t) \\ \ddot{x}_1(t) \\ \dot{x}_2(t) \\ \ddot{x}_2(t) \end{bmatrix} = \begin{bmatrix} 0 & 1 & 0 & 0 \\ -\dfrac{k_1+k_2}{m_1} & -\dfrac{c_1+c_2}{m_1} & \dfrac{k_2}{m_1} & \dfrac{c_2}{m_1} \\ 0 & 0 & 0 & 1 \\ \dfrac{k_2}{m_2} & \dfrac{c_2}{m_2} & -\dfrac{k_2}{m_2} & -\dfrac{c_2}{m_2} \end{bmatrix} \begin{bmatrix} x_1(t) \\ \dot{x}_2(t) \\ x_2(t) \\ \dot{x}_2(t) \end{bmatrix} + \begin{bmatrix} 0 & 0 \\ \dfrac{1}{m_1} & -\dfrac{1}{m_1} \\ 0 & 0 \\ 0 & \dfrac{1}{m_2} \end{bmatrix} \begin{bmatrix} F_1(t) \\ F_2(t) \end{bmatrix} \tag{3}$$

$$y = \begin{bmatrix} 1 & 0 & 0 & 0 \\ -1 & 0 & 1 & 0 \end{bmatrix} \begin{bmatrix} x_1(t) \\ \dot{x}_2(t) \\ x_2(t) \\ \dot{x}_2(t) \end{bmatrix} = \begin{bmatrix} x_1(t) \\ x_2(t) - x_1(t) \end{bmatrix}. \tag{4}$$

Intuitively, the LRA has a greater mass than the SRA, since the SRA is included in the LRA mass, thus we have a relationship with reasonable ranges of

$$m_1 = \alpha m_2, \quad \alpha \in [2, 10]\,. \tag{5}$$

To compare the stiffness of both actuators, they can be modeled as uniform bars made of the same material with elastic modulus E. Assuming the same cross sectional area A, the stiffness ratio is based on the relative length of the two actuators L_1 and L_2. Therefore, the relationship between stiffness coefficients is given by

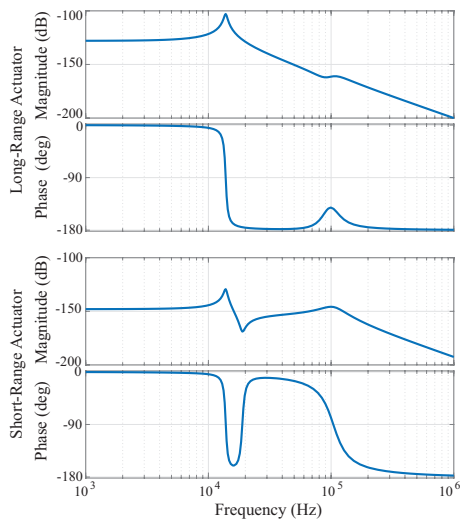

Figure 3. Frequency response of the system provided in (3)-(4).

Table 1. Parameter values of the generic dual-stage system

	LRA	SRA	
m [kg]	0.01	0.003	$\alpha = 3.33$
k [N/m]	2500000	25000000	$\beta = 0.1$
c	10	100	$\gamma = 0.1$

$$k_1 = \frac{AE}{L_1}, \quad k_2 = \frac{AE}{L_2}, \quad \rightarrow k_1 = \beta k_2, \quad \beta \in \left[\frac{1}{20}, \frac{1}{2}\right] \tag{6}$$

Determining the damping coefficients as an explicit function is challenging because they depend on the material, the shape of the structure, the boundary conditions, environmental parameters, etc., and is typically an empirically modeled parameter. Based on the authors' experience with these types of systems, it can be assumed that the relationship between the damping coefficients present in the dual-stage nanopositioner is captured by

$$c_1 \approx \gamma c_2, \quad \gamma \in \left[\frac{1}{500}, \frac{1}{10}\right]. \tag{7}$$

Frequency response (magnitude and phase) of a generic dual-stage system is shown in Fig. 3. Specifically, the top plot shows the LRA's response $y_1 = x_1$ to the LRA input F_1 and the bottom plot shows the SRA's response $y_2 = x_2 - x_1$ to the SRA input F_2. The parameter values of the generic model are shown in Tab. 2. From the figures, the resonant peak of the LRA occurs at 10 kHz in Fig. 3 (top), while the SRA has resonant and anti-resonant peaks at 10 kHz and 20 kHz in Fig. 3 (bottom). This shows the mechanical coupling between the systems. The SRA also has a peak at 100 kHz. The coupling effect is to be expected in this system since any displacement created in the LRA will cause displacement in the SRA and vice versa, although the effect of SRA inputs on the LRA are smaller as seen in the figures. The condition number of the state matrix A, defined as

$$cond(A) = \frac{|\lambda_{max}|}{|\lambda_{min}|}, \tag{8}$$

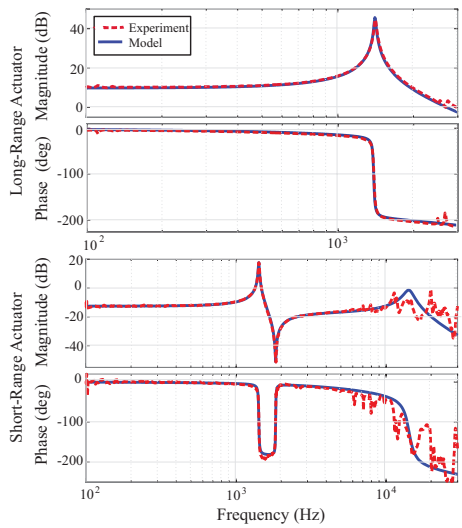

Figure 4. Red dashed line: Experimental frequency response. Blue solid line: frequency response of the fitted transfer function obtained by using least square fitting tool in MATLAB. Model taken from Mitrovic et al. (2017).

where λ_{max} is the largest eigenvalue of the matrix A, and λ_{min}, the smallest, for the values in Table 1 is 1.23×10^{10}. This high condition number is a consequence of the multiple time scales present in the system.

2.2 Experimental dual-stage model

In this paper, we use an experimentally derived model of a physical dual-stage nanopositioning system in order to simulate our response. The experimental frequency response is shown in Fig. 4 – note that they have a similar shape to the frequency response in Fig. 3. These frequency responses were experimentally obtained using both a capacitive sensor (AD Technologies 4800) and a laser vibrometer (Polytech CLV 700) and a dynamic signal analyzer (Stanford Systems SR785). To avoid hysteresis, the system was excited with sinusoidal inputs with relatively small amplitudes. Creep present in this type of actuator is minimized by recording frequency responses in frequency ranges where creep is negligible, specifically 100 Hz - 5 kHz for the LRA and 100 Hz - 20 kHz for the SRA.

For comparison, the equivalent lumped parameter values of this model were calculated. The stiffness coefficient k is calculated from the "stiffness line" which represents the asymptote preceding the natural frequency, identified from the Bode plots shown in Fig. 4, while the damping coefficient c is calculated using the "half power" method (Wu 2015). The identified values are shown in Table 2, where α, β and γ satisfy the the Eqns. 5, 6 and 7, respectively.

Transfer function models were fit to the frequency response having the form

$$G(s) = K \frac{\prod_{i=1}^{m} s - z_i}{\prod_{j=1}^{m} s - p_j}, \tag{9}$$

where s is the Laplace variable, K is the static gain, z_i is one of m zeros and p_i is one of n poles. The numerical

Table 2. Parameter values of the experimental dual-stage system

	LRA	SRA	
m [kg]	0.05	0.01	$\alpha = 5$
k [N/m]	2	5.62	$\beta = 0.35$
c	0.04	0.45	$\gamma = 0.09$

values were identified using a least square fitting method in MATLAB and are presented in Table 3 and plotted in blue in Fig. 4.

Table 3. GAINS, POLES AND ZEROS OF THE DUAL-STAGE SYSTEM

	LRA	SRA
Gain K	3.06×10^{10}	5.91×10^{11}
Poles	$-10.539 \pm i1407.9$	$-966.6 \pm i14216$
	-5000	$-8.812 \pm i1421.2$
		-20736
Zeros	N/A	$-7.1561 \pm i1837$

Note the coupling between the LRA and the SRA, which is most easily seen in the SRA frequency response in Fig. 4 (bottom plot). The first resonant peak at 1300 Hz represents coupling between the two actuators, and comes from the resonant peak from the LRA, as seen in Fig. 4 (top plot). The second resonant peak at 18 kHz actually represents the SRA dynamics. Thus, the SRA frequency response captures the SRA dynamics and the coupling effects between the actuators. The coupling effects and the actuator's actual dynamics have different time scales, and therefore can be separated using a multi-time scale approach.

2.3 Condition number

The condition number for the experimental SRA model was found to be $cond(SRA) = 14.5902$. The condition number of a matrix measures how sensitive the output is to perturbations in the input due to round-off errors made during the solution seeking process. High condition numbers may cause problem in numerical solutions, which are often sought using various software tools, which use different numerical methods such as Newton-Raphson and Runge-Kutta. Convergence to a solution for most algorithms requires mathematical manipulations such as matrix inversion. As those numerical algorithms are iterative, round-off errors through each iteration accumulate, which might lead to invalid solutions. Ideally, the condition number is 1. As the number becomes large, precision of numerical calculations is reduced. While the condition number for this system is not overly large, in practice this can lead to issues, i.e., errors in standard Matlab algorithms like those used to determine controllability and observability.

3. MULTI-TIME SCALE CONTROL

Based on the experimental model introduced above, the SRA represents an ideal system for multi-time scale control because it includes complicated dynamics, a large matrix spectrum (e.g., multi-time scales), and coupled dynamics

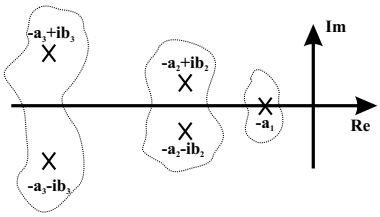

Figure 5. Pole locations determine the time scales.

between the LRA and the SRA. The experimentally fitted SRA transfer function can be represented as a state-space model, and using this model, the controllability and observablity of the system can be studied. It is interesting to see that, even though the physical systems are in fact controllable and observable, standard numerical techniques e.g., in Matlab, determine the system to be neither controllable nor observable due to the system's poor-conditioning. Changing the algorithm tolerance can sometimes solve the issue, but regardless, complex and coupled dynamics can lead to difficulties when designing standard controllers.

Multi-time scale techniques developed in Radisavljevic et al. (2019) are well suited for this type of system. This technique divides the modal form into several subsystems that are well-conditioned. In this paper, the technique is simplified because the SRA transfer function can be represented in an already decoupled form as three separate subsystems which can be independently controlled and/or observed.

The time scales are determined based on pole locations in the SRA transfer function model, as seen in Fig. 5. The first time scale, that corresponds to slow dynamics, is represented with a real pole a_1. The second time scale corresponds to fast dynamics, and is shown with a set of complex-conjugate poles $-a_2 \pm ib_2$, while the third time scale represents very fast dynamics, and is shown with a second set of complex-conjugate poles $-a_3 \pm ib_3$.

The modal form of the system is

$$\begin{bmatrix}\dot{x}_1(t)\\ \dot{x}_2(t)\\ \dot{x}_3(t)\end{bmatrix} = \begin{bmatrix}\boxed{A_1} & \mathbf{0} & \mathbf{0}\\ \mathbf{0} & \boxed{A_2} & \mathbf{0}\\ \mathbf{0} & \mathbf{0} & \boxed{A_3}\end{bmatrix}\begin{bmatrix}x_1(t)\\ x_2(t)\\ x_3(t)\end{bmatrix} + \begin{bmatrix}\boxed{B_1}\\ \boxed{B_2}\\ \boxed{B_3}\end{bmatrix} u(t) \tag{10}$$

$$y(t) = \begin{bmatrix}\boxed{C_1} & \boxed{C_2} & \boxed{C_3}\end{bmatrix}\begin{bmatrix}x_1(t)\\ x_2(t)\\ x_3(t)\end{bmatrix} \tag{11}$$

Note that the SRA system poles are complex values $p_i = a_i \pm ib_i$, given in Table 3, so the general modal form of the SRA system state matrix A takes the following form

$$\mathbf{A} = \begin{bmatrix}\boxed{A_1} & \mathbf{0} & \mathbf{0}\\ \mathbf{0} & \boxed{A_2} & \mathbf{0}\\ \mathbf{0} & \mathbf{0} & \boxed{A_3}\end{bmatrix} = \begin{bmatrix} a_1 & 0 & 0 & 0 & 0\\ 0 & a_2 & b_2 & 0 & 0\\ 0 & -b_2 & a_2 & 0 & 0\\ 0 & 0 & 0 & a_3 & b_3\\ 0 & 0 & 0 & -b_3 & a_3\end{bmatrix} \tag{12}$$

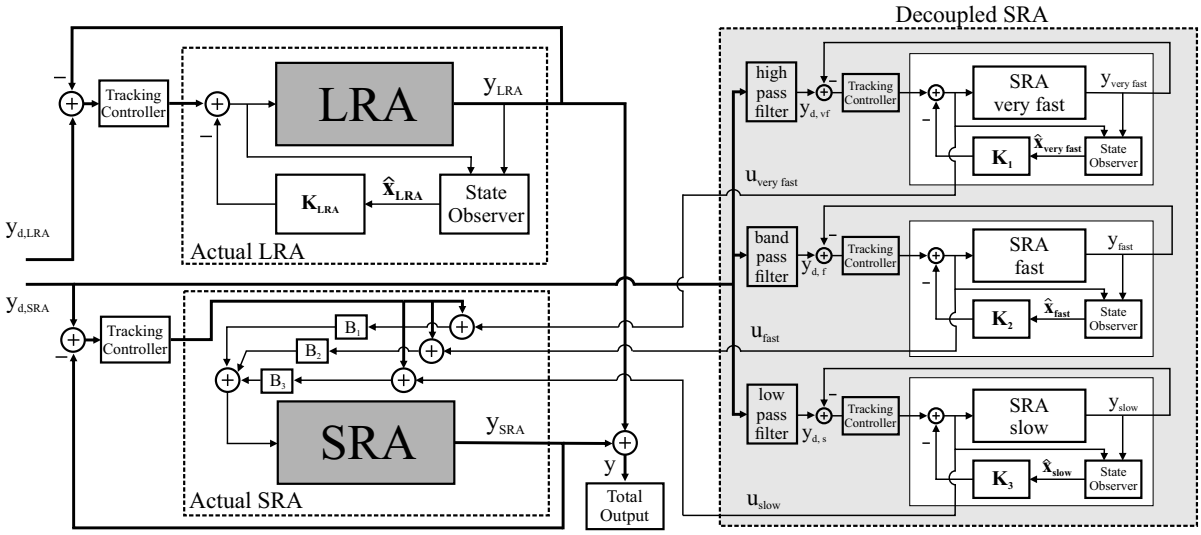

Figure 6. Multi-time scale control architecture. Decoupled SRA block has three subsystems connected in parallel, where very fast, fast and slow subsystems are controllable and observable. Calculated control inputs are used as feedforward control signal to the original SRA system, where tracking controller is used for corrections. The LRA system is controllable and observable, so analogue architecture can be constructed without decoupling.

Each of the block matrices A_1, A_2 and A_3 on the main diagonal of matrix A represents different time scales present in the original system: A_3 very fast, A_2 fast and A_1 slow dynamics. Since each triplet $(A_i, B_i, C_i)\,, i = 1, 2, 3$ is controllable and observable, state feedback with Luenberg observers can be constructed as in Fig. 6. The condition number of each subsystem equals 1, meaning that all subsystems are well-conditioned. The control scheme in Fig. 6 shows decoupled systems for online calculation of a feedforward input. The feedforward input is supplemented with a tracking controller which uses the output measurement. The tracking controller is a PID controller tuned to provide necessary robustness and error reduction.

4. SIMULATIONS

The modal form equivalent to Eqn. 10 and 11 with values for the experimentally obtained model is

$$\begin{bmatrix}\dot{x}_1(t)\\ \dot{x}_2(t)\\ \dot{x}_3(t)\\ \dot{x}_4(t)\\ \dot{x}_5(t)\end{bmatrix} = 10^4 \begin{bmatrix}-2.0736 & 0 & 0 & 0 & 0\\ 0 & -0.09666 & 1.4216 & 0 & 0\\ 0 & -1.4216 & -0.09666 & 0 & 0\\ 0 & 0 & 0 & -0.0008812 & 0.14212\\ 0 & 0 & 0 & -0.14212 & -0.0008812\end{bmatrix} \begin{bmatrix}x_1(t)\\ x_2(t)\\ x_3(t)\\ x_4(t)\\ x_5(t)\end{bmatrix} + \begin{bmatrix}0.722409\\ -0.277630\\ 0.523323\\ -0.000039\\ 0.000686\end{bmatrix} u(t) \tag{13}$$

$$y(t) = 10^5 \left[0.013843\ 0.028369\ -0.003839\ 1.961667\ -0.05548\right] \left[x_1(t)\ x_2(t)\ x_3(t)\ x_4(t)\ x_5(t)\right]^T \tag{14}$$

where each subsystem's controllability and observability matrices have full rank. State feedback controllers and observers are determined by pole-placement

$$\left.\begin{aligned} \text{very fast SRA FB:}\quad & K_1 = 365.4438759\\ \text{fast SRA FB:}\quad & K_2 = 10^4 \begin{bmatrix}-2.6774998\\ 2.2229565\end{bmatrix}\\ \text{slow SRA FB:}\quad & K_3 = 10^7 \begin{bmatrix}2.4319584\\ 1.6447982\end{bmatrix}\end{aligned}\right\} \tag{15}$$

$$\left.\begin{aligned} \text{very fast SRA observer:}\quad & L_1 = 60.8705069\\ \text{fast SRA observer:}\quad & L_2 = \begin{bmatrix}43.7415717\\ 54.7641023\end{bmatrix}\\ \text{slow SRA observer:}\quad & L_3 = \begin{bmatrix}0.3310440\\ 2.38049758\end{bmatrix}\end{aligned}\right\} \tag{16}$$

The LRA state-space matrix triplet $(A_{LRA}, B_{LRA}, C_{LRA})$ does not suffer from the same issues as the SRA and is controllable and observable. Thus the controller and observer for this stage is designed using standard methods and is shown in Fig. 6. State feedback controller and observer gains are:

$$\begin{aligned} \text{LRA FB gain:}\quad & K_{LRA} = 10^{11} \begin{bmatrix}0.0000025\\ 0.0063647\\ 2.5586978\end{bmatrix}^T\\ \text{LRA observer gain:}\quad & L_{LRA} = 10^2 \begin{bmatrix}-5.8334994\\ 0.0031525\\ 0.0000004\end{bmatrix}\end{aligned} \tag{17}$$

In order to split the signal between the three time-scales, three first-order analogue filters are used. A low-pass filter with cutoff frequency at 450 Hz is designed for the low-speed dynamics, a band-pass filter with pass band of 300-2500 Hz is used for the fast dynamics, and a high-pass with cutoff frequency at 4000 Hz is designed for the very fast dynamics. Bode plots of the designed filters are shown in Fig. 7. The idea behind these filters is to split the SRA reference signal into three separate signals with corresponding frequencies to the dynamics of each

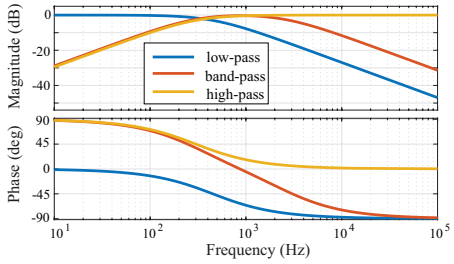

Figure 7. Three filters used to split the SRA reference signal between the corresponding frequencies to the dynamics of each subsystem.

subsystem. By doing this, it is assured that each subsystem operates in its most fitting frequency regime.

The performance of the closed-loop system can be quantified by comparing the open- and closed-loop response of the individual states. The Bode plots in Fig. 8 show open-loop and closed-loop frequency responses for the LRA and SRA, respectively. Both closed-loop LRA and SRA systems achieve closed-loop bandwidths of 200 Hz for the LRA and 900 Hz for the SRA, which are significantly higher than open-loop bandwidths (90 Hz for the LRA, and 300 Hz for the SRA).

Two individual trajectory tracking examples are also presented. First, Fig. 9 (top) shows tracking results for a reference trajectory $y_d = 2sin(2\pi 100t)$. The maximum displacement of the LRA is approximately ± 9.75 μm, while the SRA has maximum displacement of approximately ± 0.75 μm. Therefore, the desired amplitude of the SRA is chosen to be 0.5 μm in order to fully utilize this actuator (without saturating it), and the LRA trajectory handles the rest of the desired input trajectory, that is 1.5 μm. Individual LRA and SRA signals and their corresponding errors are shown in Fig. 9 (middle and bottom).

The individual signals coming from the decoupled SRA system $y_{veryfast}$, y_{fast} and y_{slow} are shown in Fig. 10. The signals are split such that the largest amplitude is handled by the slow dynamics, while smaller amplitudes are handled by the fast and very fast dynamics. It is

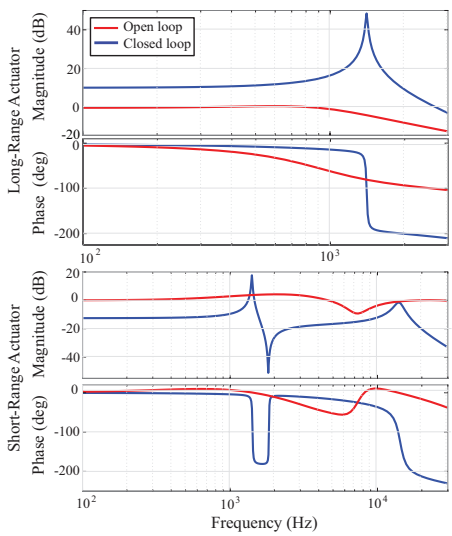

Figure 8. Open loop and closed loop Bode diagram for the LRA and the SRA.

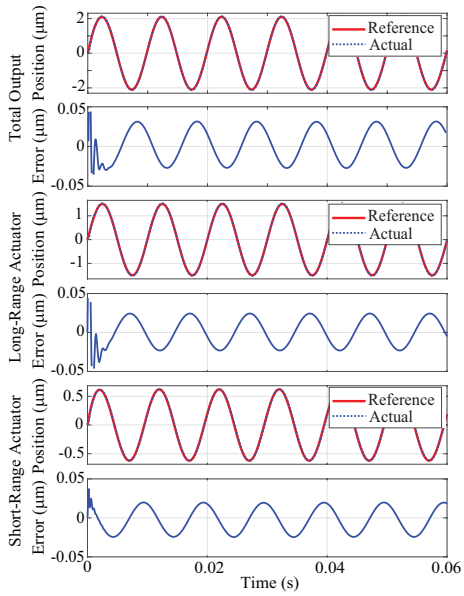

Figure 9. (top) Total output and tracking error when reference signal is a sinusoid of frequency 100 Hz and amplitude 1.5 μm for the LRA and 0.5 μm for the SRA. (middle and bottom) Individual LRA and SRA references and corresponding tracking errors.

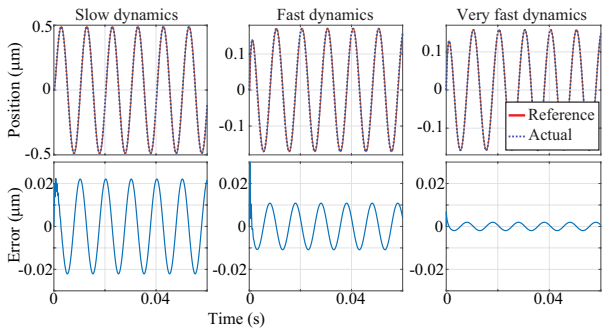

Figure 10. Signals coming from the decoupled SRA dynamics: (top) desired and achieved signals; (bottom) error signals.

possible to change the portion of the signal that is being diverted to each subsystem by varying the cutoff frequencies of the low-pass, band-pass and high-pass filters. The control signals calculated for each subsystem are added, and applied as a feedforward control action to the SRA.

The root mean square error is calculated as

$$RMSE = \sqrt{\frac{\sum_{i=1}^{n}(y_d - y)^2}{n}} \tag{18}$$

where y_d is the desired trajectory $y_d = y_{d,LRA} + y_{d,SRA}$, y is the achieved trajectory, and n represents the length of the signal vectors. The RMSE value for the LRA trajectory is 2.83×10^{-4}, for the SRA is 1.43×10^{-4}, for the total output 1.52×10^{-4}, and for all three trajectories the error is approximately less than 2%.

A 50 Hz triangular trajectory is also explored as shown in Fig. 11. In both cases, the LRA and SRA tracking error is sufficiently small (less than 2%), where the RMSE value for the LRA trajectory is 5.33×10^{-4}, for the SRA is 0.23×10^{-4}, and for the total output 5.56×10^{-4}.

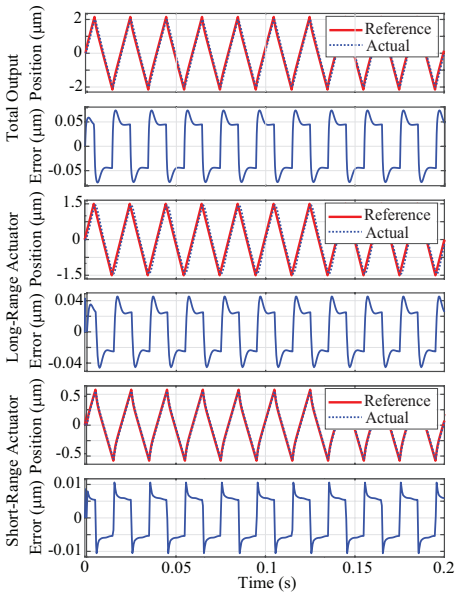

Figure 11. (top) Tracking reference and corresponding tracking error signal of the controlled system with triangular signal as reference trajectory with amplitude of 2 μm and frequency 50 Hz. (middle and bottom) LRA and SRA tracking performance for triangular reference trajectory.

5. CONCLUSIONS

In this paper, the multi-time scale control approach is applied to a dual-stage nanopositioning system. The presented approach provides a new concept in the area of dual-stage system control. The multi-time scale nature of the analyzed nanopositioning system is a result of coupling and interaction between the two actuators, LRA and SRA. For this specific type of the system, multi-time scale control technique design was shown to be effective and the obtained simulation results display high-precision tracking with error less than 2% for different input signals. The results provide a solid ground for future applications and further experimental study which is in the scope of our research group.

REFERENCES

Butler, H. Position Control in Lithographic Equipment [Applications of Control]. *IEEE Control Systems Magazine*, volume 31, pages 28–47, 2011.

Horowitz, R., Li, Y., Oldham, K., Kon, S., and Huang, X. Dual-Stage servo systems and vibration compensation in computer hard disc drives. *Control Engineering Practice*, volume 15, pages 291–305, 2007.

Escareno, J. A., Abadie, J., Rakotondrabe, M. Robust micro-positioning control of a 2DOF piezocantilever based on an extended-state LKF

Fleming, A. J. Dual-stage vertical feedback for high-speed scanning probe microscopy. *IEEE Transactions on Control Systems Technology*, volume 19, pages 156–165, 2011.

Fleming, A.J., and Leang, K.K. Design, Modeling and Control of Nanopositioning Systems. *Springer International Publishing* 978-3-319-06616-5, 2014.

Ito, S.,Neyer, D., Steininger, J., and Schitter, G. Dual Actuation of Fast Scanning Axis for High-speed Atomic Force Microscopy. *IFAC-PapersOnLine*, volume 50, pages 7633–7638, 2017.

Ojalvo, I.U. Interpretation and Solution of Ill-Conditioned Equations Arising in Parameter Estimation and System Identification. *Mathematical and Computer Modeling*, volume 14, pages 209–212, 1990.

Peters, G., and Wilkinson, J.H. Inverse Iteration, Ill-Conditioned Equations and Newton's Method. *SIAM Review*, volume 21, pages 339–360, 1978.

Kalyanam, K., Tsao, T. Two-period repetitive and adaptive control for repeatable and nonrepeatable runout compensation in disck drive track following. *Transactions on Mechatronics*, volume 17, pages 756–766, 2012.

Tuma, T., Haeberle, W., Rothuizen, H., Lygeros, J., Pantazi, A., and Sebastian, A. Dual-Stage Nanopositioning for High-Speed Scanning Probe Microscopy. *IEEE/ASME Transactions on Mechatronics*, volume 19, pages 1035–45, 2014.

Milanovic, M., Radisavljevic-Gajic, V. Multi-Timescale-Based Partial Optimal Control of a Proton-Exchange Membrane Fuel Cell. *Energies*, volume 13, pages 166, 2020.

Mitrovic, A., Leang, K.K., and Clayton, G.M. Spatial filter design for dual-stage systems. *ASME 2017 Dynamic Systems and Control Conference*, DSCC2017-5347, 2017.

Radisavljevic-Gajic, V., Milanovic, M., and Rose, P. Multi-Stage and Multi-Time Scale Feedback Control of Linear Systems with Applications to Fuel Cells. *Springer International Publishing*, 978-3-030-10388-0, 2019.

Radisavljevic-Gajic, V., Milanovic, M., and Clayton, G.M. Three-stage feedback controller design with applications to three time-scale linear control systems. *Journal of Dynamic Systems, Measurement, and Control*, volume 139, 2017.

Rezac, M., Hurak, Z. Structured MIMO H_∞ design for dual-stage inertial stabilization: Case study for HIFOO and Hinfstruct solvers. *Mechatronics*, volume 23, pages 1084–1093, 2013.

Schroeck,S. J., Messner, W. C., McNab, R. J. On compensator design for linear time-invariant dual-input single-output systems. *IEEE/ASME Transactions on Mechatronics*, volume 6, pages 50–57, 2001.

Wang, Z., Pannier, C. P., Barton, K., Hoelzle, D. J. Application of robust monotonically convergent spatial iterative learning control to microscale additive manufacturing. *Mechatronics*, volume 56, pages 157–165, 2018.

Wu, B. A correction of the half-power bandwidth method for estimating damping. *Arch. Applied Mechanics*, volume 85, pages 315–320, 2015.

Zhang, Y., Yan, P. An adaptive integral sliding mode control approach for piezoelectric nano-manipulation with optimal transient performance. *Mechatronics*, volume 52, pages 119-126, 2018.

Zundert, J. van, Oomen, T., Verhaegh, J., Aangenent, W., Antunes, D. J., Heemels, W.P.M.H. Beyond performance/cost tradeoffs in motion control: a multirate feedforward design with application to a dual-stage wafer system. *IEEE Transactions on Control Systems Technology*, volume -, pages 1–14, 2018.